Transp Porous Med (2009) 77:243–265
DOI 10.1007/s11242-008-9306-9

The Onset and Nonlinear Development of Vortex Instabilities in a Horizontal Forced Convection Boundary Layer With Uniform Surface Suction

D. A. S. Rees

Received: 6 October 2008 / Accepted: 6 November 2008 / Published online: 3 December 2008

Abstract We consider the flow and heat transfer caused by a strong external flow passing over a hot surface with uniform surface suction. When the Péclet number based on the external velocity is sufficiently large, the resulting thermal boundary layer develops in a nonsimilar manner until it attains an asymptotic state which is independent of the streamwise coordinate, x, when it is dominated by the surface suction. For sufficiently large, but moderate, values of the Darcy–Rayleigh number this boundary layer becomes unstable to streamwise vortex disturbances. We employ a parabolic solver to determine how such disturbances, when placed very close to the leading edge, evolve with distance downstream. Neutral stability is then defined to be when a suitable energy functional ceases to decay/grow as x increases. Thus a neutral curve may be mapped out based upon the behaviour of this functional. Given that the uniform asymptotic state is well known to admit subcritical instabilities, our linearised analysis is extended into the nonlinear domain and the effect of different magnitudes of disturbance is ascertained. It is found that a surprisingly rich variety of vortex pattern emerges which is sometimes sensitively dependent on the values of the governing parameters. These patterns include wavy vortices and abrupt changes in perceived wavelength.

Keywords Forced convection · Surface suction · Thermoconvective instability · Vortices

Nomenclature

A Amplitude of disturbance
c Constant
E Energy functional
g Acceleration due to gravity
k Vortex wavenumber
K Permeability

D. A. S. Rees (✉)
Department of Mechanical Engineering, University of Bath, Bath BA2 7AY, UK
e-mail: ensdasr@bath.ac.uk

L	Length scale
N	Number of modes in the nonlinear analysis
p, P	Pressure
Pe	Péclet number
q	Modal surface rate of heat transfer
Q	Surface rate of heat transfer defined in Eq. (44)
Ra	Darcy–Rayleigh number
T	Temperature
T_{w}	Surface temperature
T_∞	Ambient temperature
u, v, w	Velocities in the x, y and z directions, respectively
U	External velocity
W	Suction velocity
x	Horizontal streamwise coordinate
X	Scaled form of x
y	Horizontal spanwise coordinate
z	Vertical coordinate

Greek letters

α	Thermal diffusivity
β	Coefficient of thermal expansion
η	Similarity variable
θ	Nondimensional temperature
Θ	Temperature perturbation for linearised analysis
μ	Dynamic viscosity
ξ	Scaled horizontal coordinate
ρ	Reference density
χ	Dummy variable
ψ	Streamfunction

Subscripts and superscripts

$\bar{}$	Dimensional
$\hat{}$	Nondimensional
b	Referring to basic state
c	Critical
i	Initiation (referring to location of the disturbance)
n	Mode number
0, 1, 2, ...	Mode numbers

1 Introduction

We consider the instability of the forced convection thermal boundary layer which is formed near a semi-infinite, uniformly hot permeable surface which bounds a semi-infinite domain. The permeable surface is modelled by imposing a uniform suction velocity at that surface. We assume that the magnitude of the external stream is much greater than that of the suction

velocity, and therefore the resulting thermal boundary layer is, at least initially, of Graetz type (i.e. a forced convection flow past a discontinuous change in a temperature boundary condition). The effect of suction becomes dominant further downstream and the boundary layer eventually attains a constant thickness. However, we retain the buoyancy term in the governing equations and although the buoyancy correction to the externally imposed flow is asymptotically small when the Péclet number is asymptotically large, its presence allows the possibility of thermoconvective instability. We note that, although our study uses the language of heat transfer, our analysis could also apply to solutal convection such as the saline boundary layer which is formed beneath the surface of an evaporating salt lake.

Wooding (1960) was the first person to consider how the effect of a uniform seepage through a permeable boundary affects the criterion for the onset of convection in the presence of density inversion. By considering a semi-infinite domain with warmer fluid rising towards an cold permeable surface, he showed that the thermal field takes a decaying exponential form and he also provided a linearised stability analysis of this state. Termed the Wooding problem by Pieters and Schuttelaars (2008), it has been extended in a variety of directions in subsequent years. For example, Sutton (1970) computed the effect of relatively weak suction within a porous layer of finite height heated from below, while the effect of different types of boundary conditions were considered in detail by Jones and Persichetti (1986) and Nield (1986). On the other hand, the combined effect of inclination and anisotropy was considered by Rees and Storesletten (2002) who delineated regions in parameter space where either longitudinal rolls or transverse rolls may be found as the primary mode of instability. In other articles, Nield (1998) considered an inclined temperature gradient which generates an additional horizontal velocity field, Shivakumara (1999) and Khalili and Shivakumara (2003) considered non-Darcy effects, Khalili and Shivakumara (1998) and Yoon et al. (1998) included internal heat generation, Khalili et al. (2003) allowed for superposed fluid and porous layers, Shivakumara and Khalili (2001) introduced a second diffusing component, while Shivakumara and Sureshkumar (2007, 2008) analysed different non-Newtonian fluids. All these latter articles were confined to linearised theory.

As pointed out by Pieters and Schuttelaars (2008), the Wooding problem differs in its nature from the Horton–Rogers–Lapwood (or Darcy–Bénard) problem by being non-self-adjoint. Indeed, the Darcy–Bénard problem always admits supercritical bifurcations to a strongly convecting state, while the Wooding problem has a significant branch of deeply subcritical solutions. There have also been numerous studies on the nonlinear aspects of the Wooding problem. Homsy and Sherwood (1976) performed both a linear stability analysis and a nonlinear energy analysis in a layer of finite height. A more thorough examination of various stability theories was carried out by van Duijn et al. (2002) who also considered the temporal approach of the basic state towards the steady exponentially decaying boundary layer. Both van Duijn et al. (2002) and Alloui et al. (2005) present some time-dependent numerical simulations, although the latter authors also consider fixed-flux boundary conditions. We also note the detailed analysis of the stability boundaries of hexagonal convection given by Riahi (1989).

The aim of this article is to extend the Wooding problem to one where there is a strong horizontal flow present, such as would arise with a suitably large horizontal pressure gradient imposed. This would cause a thermal boundary layer to form which is identical to the Wooding problem at sufficiently large distances from the leading edge, apart from the strong streamwise velocity component, but the region relatively close to the leading edge is one where suction is subdominant, and therefore the thermal boundary layer is very much like the porous medium analogue of the Graetz problem. This thermal boundary layer is of forced convective type since a suitably defined Péclet number is large, but it is nevertheless subject to

instability should the Darcy–Rayleigh number be sufficiently large. We will consider convective instabilities of the form of streamwise vortices and will present both a linearised analysis and some representative nonlinear computations. This flow problem bears some resemblance to the salt lake problem of Wooding et al. (1997a,b) and Wooding (2007), although the magnitude of the external flow is substantially smaller than in this article, and the present analysis is three-dimensional.

Near the leading edge, the linearised stability equations, which take the form of parabolic partial differential equations, are identical to those solved by Selim and Rees (2007a) in their study of an impulsively heated thermal boundary layer without an imposed horizontal flow. Indeed, the time variable τ which is used by Selim and Rees (2007a) plays exactly the same role as the spatial variable, ξ, which is employed here. Although this analogy breaks down when disturbances enter the nonlinear regime, we nevertheless expected much of the qualitative nature of the unsteady problem of Selim and Rees (2007a) to carry over to the present configuration. The study of the stability of such nonsimilar boundary layers is one where there remains much interest and activity, some examples of which are the recent articles by Ennis-King et al. (2005) on anisotropic media, Kim et al. (2008) on the melting of ice within a porous medium, Riaz et al. (2006) who also present some detailed nonlinear simulations and Nouri-Borujerdi et al. (2007) on the effects of local thermal non-equilibrium. However, there remains some differences of opinion in the literature about the best way of defining instability. A detailed account of these matters may be found in the review articles by Rees (1998, 2002) and Rees et al. (2008b). In summary, it is argued that the natural evolution of disturbances (either spatially for a steady basic state, or in time for an unsteady basic state) should be used for determining stability criteria, rather than by imposing specific criteria, such as the setting of the time derivative of the whole temperature profile to zero. In general, the former method yields earlier stability criteria than the latter method, because the latter method imposes strict contraints on the behaviour of the disturbances that are not there in practice. In a further argument, Storesletten and Rees (1998) argue that the critical distances obtained for many boundary layer flows are far too small for the boundary layer approximation to be valid. It was this observation that motivated the analysis of Rees (2001) who considered free convection from a nearly vertical heated surface where the critical distance is asymptotically large, and therefore the analysis remains self-consistent. The implication of the work of Rees (2001) is that instability analyses of boundary layers at $O(1)$ angles are inherently inconsistent, and that the only consistent analysis would involve the fully elliptic system of equations.

Finally, it is necessary to mention that there also exist two articles which consider the combination of a boundary layer flow and surface suction in porous media; these are the works of Jang et al. (1995) and Hassanien et al. (2004). In the former article, a variable suction is employed but the disturbances are assumed to have a zero x-derivative at onset. Moreover, their mixed convection parameter is assumed to be a constant, whereas its definition exhibits a clear streamwise variation. In the latter article, a power law variation in surface temperature is employed together with a varying suction velocity. However, the Forchheimer terms are not written in a frame invariant form, and it is therefore difficult to assess how accurate their results are.

2 Basic Equations and Flow

A semi-infinite porous region is bounded below by the horizontal surface $\bar{z} = 0$ and is unbounded above. The surface at $\bar{z} = 0$ is permeable and forms a suction surface, where the

vertical velocity $\bar{w} = -W$, is maintained, and where $W > 0$ is a constant. In addition, a horizontal flow of magnitude, $U(\gg W)$, is induced by a uniform pressure gradient in the $\bar{x}$-direction. Gravity acts in the negative $\bar{z}$-direction. The ambient temperature of the porous medium is T_∞, while that part of the bounding surface which lies in the range $\bar{x} > 0$ is held at the higher temperature T_w.

It is assumed that Darcy's law is applicable, that the medium is isotropic and homogeneous, that the phases are in local thermal equilibrium and that the Boussinesq approximation is valid. The governing steady-state equations are now given by,

$$\frac{\partial \bar{u}}{\partial \bar{x}} + \frac{\partial \bar{v}}{\partial \bar{y}} + \frac{\partial \bar{w}}{\partial \bar{z}} = 0, \tag{1}$$

$$\bar{u} = -\frac{K}{\mu}\frac{\partial \bar{p}}{\partial \bar{x}}, \tag{2}$$

$$\bar{u} = -\frac{K}{\mu}\frac{\partial \bar{p}}{\partial \bar{y}}, \tag{3}$$

$$\bar{w} = -\frac{K}{\mu}\left[\frac{\partial \bar{p}}{\partial \bar{z}} - \rho g \beta (T - T_\infty)\right], \tag{4}$$

$$\alpha\left[\frac{\partial^2 T}{\partial \bar{x}^2} + \frac{\partial^2 T}{\partial \bar{y}^2} + \frac{\partial^2 T}{\partial \bar{z}^2}\right] = \bar{u}\frac{\partial T}{\partial \bar{x}} + \bar{v}\frac{\partial T}{\partial \bar{y}} + \bar{w}\frac{\partial T}{\partial \bar{z}}, \tag{5}$$

where all terms are defined in the Nomenclature. The boundary conditions are

$$\bar{z} = 0: \quad \bar{w} = -W, \quad T = \begin{cases} T_\infty (\bar{x} < 0) \\ T_\mathrm{w} (\bar{x} > 0) \end{cases}, \quad \bar{z} \to \infty: \quad T \to T_\infty. \tag{6}$$

In addition, when $\bar{x}$ is large and negative, all quantities should be at their ambient values, namely $\bar{u} = U$, $\bar{v} = 0$, $\bar{w} = -W$ and $T = T_\infty$. The nature of this problem is such that the boundary layer approximation will be valid and the governing equations become parabolic in $\bar{x}$, and therefore no large-$\bar{x}$ boundary conditions are required.

Far from the leading edge (i.e. for $\bar{x}$ sufficiently large and positive), it is straightforward to show that

$$\bar{u} = U, \quad \bar{w} = -W, \quad \text{and} \quad T = T_\infty + (T_\mathrm{w} - T_\infty)\exp(-W\bar{z}/\alpha), \tag{7}$$

and therefore α/W may be used as a natural lengthscale in order to nondimensionalise the equations. On setting $L = \alpha/W$, the following substitutions are introduced:

$$(\bar{x}, \bar{y}, \bar{z}) = L(x, y, z) \quad (\bar{u}, \bar{v}, \bar{w}) = W(\hat{u}, \hat{v}, \hat{w}) \quad \bar{p} = \frac{\mu\alpha}{K}\hat{p}, \quad T = T_\infty + (T_\mathrm{w} - T_\infty)\theta, \tag{8}$$

Hence the governing Eqs. 1–5, become,

$$\frac{\partial \hat{u}}{\partial x} + \frac{\partial \hat{v}}{\partial y} + \frac{\partial \hat{w}}{\partial z} = 0, \tag{9}$$

$$\hat{u} = -\frac{\partial \hat{p}}{\partial x}, \tag{10}$$

$$\hat{v} = -\frac{\partial \hat{p}}{\partial y}, \tag{11}$$

$$\hat{w} = -\frac{\partial \hat{p}}{\partial z} + Ra\,\theta, \tag{12}$$

$$\frac{\partial^2 \theta}{\partial x^2} + \frac{\partial^2 \theta}{\partial y^2} + \frac{\partial^2 \theta}{\partial z^2} = \hat{u}\frac{\partial \theta}{\partial x} + \hat{v}\frac{\partial \theta}{\partial y} + \hat{w}\frac{\partial \theta}{\partial z}, \tag{13}$$

where the Darcy–Rayleigh number is defined as,

$$Ra = \frac{\rho g \beta K L(T_{\mathrm{w}} - T_\infty)}{\mu \alpha} = \frac{\rho g \beta K (T_{\mathrm{w}} - T_\infty)}{\mu W}. \tag{14}$$

Given that the dimensional magnitude of the external free stream is U, the equivalent in nondimensional terms is U/W, which may be written in the form,

$$\frac{U}{W} = \frac{UL}{\alpha} = Pe, \tag{15}$$

and therefore this velocity ratio also plays the role of a Péclet number.

In this article, we shall assume that $Pe \gg 1$ and therefore the development of the temperature profile is described accurately by the boundary layer approximation. Although this would suggest that the configuration we study is of forced convective type, the Darcy–Rayleigh number is taken to be of $O(1)$, and therefore the boundary layer will be subject to thermoconvective instability when Ra is sufficiently large. Therefore we need to consider the appropriate boundary conditions for positive values of x only:

$$z = 0: \quad \hat{w} = -1, \quad \theta = 1, \qquad z \to \infty: \quad \hat{u} \to Pe, \quad \theta \to 0. \tag{16}$$

In the absence of temperature variations, the velocity and pressure fields are easily shown to be $\hat{u} = Pe$, $\hat{v} = 0$, $\hat{w} = -1$ and $\hat{p} = -Pe\,x + z$. Therefore we may perturb Eqs. 10–13 according to,

$$\hat{u} = Pe + u, \qquad \hat{v} = v, \qquad \hat{w} = -1 + w, \qquad \hat{p} = -Pe\,x + z + p, \tag{17}$$

to obtain a new set of equations with homogeneous boundary conditions. Eqs. 10– 12 remain unchanged, but Eq. 13 becomes,

$$\frac{\partial^2 \theta}{\partial x^2} + \frac{\partial^2 \theta}{\partial y^2} + \frac{\partial^2 \theta}{\partial z^2} + \frac{\partial \theta}{\partial z} - Pe\frac{\partial \theta}{\partial x} = u\frac{\partial \theta}{\partial x} + v\frac{\partial \theta}{\partial y} + w\frac{\partial \theta}{\partial z}. \tag{18}$$

Finally, we need to rewrite the governing equations in streamfunction/temperature form to allow the detailed basic state to be determined, and in pressure/temperature form in order to analyse vortex instabilities. In the former case, we may introduce the substitutions,

$$u = -\frac{\partial \psi}{\partial z}, \quad v = 0, \quad w = \frac{\partial \psi}{\partial x}. \tag{19}$$

and thus the streamfunction satisfies the equation,

$$\frac{\partial^2 \psi}{\partial x^2} + \frac{\partial^2 \psi}{\partial z^2} = Ra\,\frac{\partial \theta}{\partial x}, \tag{20}$$

while Eq. 18 becomes,

$$\frac{\partial^2\theta}{\partial x^2}+\frac{\partial^2\theta}{\partial z^2}+\frac{\partial\theta}{\partial z}-Pe\frac{\partial\theta}{\partial x}=\frac{\partial\psi}{\partial x}\frac{\partial\theta}{\partial z}-\frac{\partial\psi}{\partial z}\frac{\partial\theta}{\partial x}. \tag{21}$$

In the latter case, the three velocity components may be eliminated using Darcy's law and we obtain,

$$\frac{\partial^2 p}{\partial x^2}+\frac{\partial^2 p}{\partial y^2}+\frac{\partial^2 p}{\partial z^2}=Ra\frac{\partial\theta}{\partial z}, \tag{22}$$

$$\frac{\partial^2\theta}{\partial x^2}+\frac{\partial^2\theta}{\partial y^2}+\frac{\partial^2\theta}{\partial z^2}+\frac{\partial\theta}{\partial z}-Pe\frac{\partial\theta}{\partial x}=Ra\,\theta\frac{\partial\theta}{\partial z}-\frac{\partial p}{\partial x}\frac{\partial\theta}{\partial x}-\frac{\partial p}{\partial y}\frac{\partial\theta}{\partial y}-\frac{\partial p}{\partial z}\frac{\partial\theta}{\partial z}. \tag{23}$$

The boundary conditions are,

$$z=0: \qquad \psi=0, \quad \theta=1, \quad \frac{\partial p}{\partial z}=Ra, \tag{24}$$

$$z\to\infty: \qquad \frac{\partial\psi}{\partial z},\ \theta,\ \frac{\partial p}{\partial z}\to 0. \tag{25}$$

3 Boundary Layer Analysis and Basic State

The appropriate boundary layer scalings may be obtained by balancing the magnitudes of the θ_{zz} and $Pe\,\theta_x$ terms in Eq. 21. This yields the balance,

$$\frac{Pe\,z^2}{x}=O(1). \tag{26}$$

It is typical to assume that $x=O(1)$ in boundary layer theory, because this means that the distance to the leading edge is a distance of significance to the solution. However, in the present context, this means that the suction term in (21), namely the $\partial\theta/\partial z$ term, is negligible, whereas it should play an important role. Therefore it is necessary to insist that $z=O(1)$, and Eq. 26 now implies that $x=O(Pe)$. This motivates the substitution, $x=Pe\,X$, and Eqs. 20 and 21 reduce to the forms,

$$\frac{\partial^2\psi}{\partial z^2}=\frac{Ra}{Pe}\frac{\partial\theta}{\partial X}+O(Pe^{-2}), \tag{27}$$

$$\frac{\partial^2\theta}{\partial z^2}+\frac{\partial\theta}{\partial z}=\frac{\partial\theta}{\partial X}+O(Pe^{-2}). \tag{28}$$

Equation 28 shows that the evolution of θ is independent of ψ at leading order, which reflects the fact that this is a forced convection problem, or nearly so. On the other hand, Eq. 27 indicates that buoyancy induces a small, $O(Pe^{-1})$, correction to the original uniform free stream.

The appropriate similarity variable for small values of X is $z/2X^{1/2}$, where the '2' has been introduced for numerical convenience, while the one for large values of X is z itself. Therefore we shall introduce the following continuous transformation which will model both extremes well:

$$\eta=\frac{z(1+2X^{1/2})}{2X^{1/2}}, \qquad \xi=X^{1/2}. \tag{29}$$

Eq. 28 becomes,

$$(1+2\xi)^2\frac{\partial^2\theta}{\partial\eta^2}+[2\xi(1+2\xi)+2\eta]\frac{\partial\theta}{\partial\eta}=2\xi\frac{\partial\theta}{\partial\xi}. \tag{30}$$

From this equation it is clear that the first term in a Taylor series expansion of θ about $\xi = 0$ is

$$\theta=\mathrm{erfc}(\eta)=\frac{2}{\sqrt{\pi}}\int_\eta^\infty e^{-\chi^2}\,\mathrm{d}\chi, \tag{31}$$

while the corresponding large-ξ solution is

$$\theta=e^{-z}, \tag{32}$$

which is the nondimensional counterpart to the expression for T given in Eq. 6.

Equation 27, subject to the boundary conditions that $\theta = 1$ at $\eta = 0$ and that $\theta \to 0$ as $\eta \to 0$, was solved using a modified version of the Keller-box method. The most usual implementation of this method employs the reduction of the system of equations to first-order form in η, and then finite difference approximations are applied midway between each η and each ξ value, i.e. at the centre of the 'box' formed by neighbouring grid lines. The resulting finite difference equations are both nonlinear and implicit, and the solutions are obtained using a multi-dimensional Newton–Raphson technique. Although the Jacobian matrix is usually encoded within the program, we employ numerical derivatives to simplify the encoding. The method, as stated above, is of second order accuracy in both ξ and η, but it shares the same stability properties as the Crank Nicolson method in that it is A-stable, and can exhibit slowly decaying pointwise oscillations if the steplength in ξ is too large. The equivalent Backward Euler stepping is also L-stable, but is only of first-order accuracy. Therefore we have adopted the second-order BDF method (see, for example, Plato (2003), which has the advantage of being both L-stable and also retains the second-order accuracy we desired. As far as we know this is the first time that this method has been used within a Keller-box code. Extensive tests were undertaken comparing results with those of the standard central differences where baseline figures for comparison were obtained by successive interval-halving and Richardson extrapolation. It was confirmed that the method is of second-order accuracy in ξ and the data obtained often exceeds the absolute accuracy of the central–difference solution.

Figure 1 displays the isotherms of the resulting thermal boundary layer plotted in terms of X and y. Thus the evolving thickness of the boundary layer is displayed as it would appear in reality, although the horizontal coordinate has necessarily been compressed by a factor equal to the Péclet number. It is easily seen that the thickness of the boundary layer grows

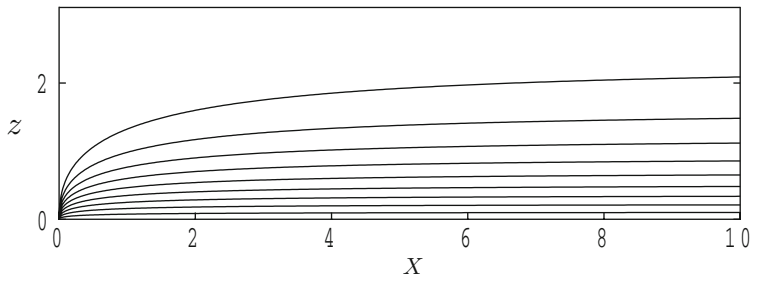

Fig. 1 Temperature field corresponding to the basic forced convection state. Isotherms are plotted at intervals of 0.1

rapidly from the state given by Eq. 31 until $X \sim 2$, after which it evolves slowly towards its asymptotic profile given by Eq. 32.

4 Linear Stability Analysis

We now introduce small-amplitude vortex disturbances near the leading edge and following their subsequent downstream evolution. The basic state we analyse for stability is now denoted by $\theta_b(\xi, \eta)$, and there will be a corresponding pressure profile, $p_b(\xi, \eta)$. However, it is not necessary to calculate this latter profile as it does not appear in the linearised stability equations. Therefore we shall introduce vortex disturbances in the following manner:

$$(p, \theta) = (p_b, \theta_b) + (P, \Theta)e^{iky}, \tag{33}$$

where both P and Θ are functions of ξ and η, and where k is the spanwise wavenumber. The following system of disturbance equations are obtained:

$$\frac{\partial^2 P}{\partial \eta^2} - k^2 \left(\frac{2\xi}{1+2\xi}\right)^2 P = Ra\left(\frac{2\xi}{1+2\xi}\right)\frac{\partial \Theta}{\partial \eta}, \tag{34}$$

$$\frac{\partial^2 \Theta}{\partial \eta^2} + \left[\frac{2\xi}{1+2\xi} + \frac{2\eta}{(1+2\xi)^2}\right]\frac{\partial \Theta}{\partial \eta} - k^2\left(\frac{2\xi}{1+2\xi}\right)^2 \Theta + \left[\frac{\partial P}{\partial \eta} - Ra\left(\frac{2\xi}{1+2\xi}\right)\theta\right]\frac{\partial \theta_b}{\partial \eta} = \frac{2\xi}{(1+2\xi)^2}\frac{\partial \Theta}{\partial \xi}. \tag{35}$$

At sufficiently large values of ξ, the asymptotic state where the boundary layer has constant thickness is attained, the last term in Eq. 35 then becomes negligible, and all coefficients become independent of ξ. Consequently, an ordinary differential system is obtained for the disturbances which corresponds precisely to the problem studied by Wooding (1960), where the stability of an identical suction-induced boundary layer was studied in the absence of an external stream. In the present notation, it is straightfoward to determine that the critical Darcy–Rayleigh number is 14.3552 with corresponding wavenumber, $k_c = 0.7589$, with all quoted significant figures being correct. Lower values of Ra will result in a boundary layer that is thermoconvectively stable to all small-amplitude disturbances.

It is possible to define a local Rayleigh number, Ra_{loc}, based upon the local boundary layer thickness (say the $\theta_b = 0.1$ isotherm shown in Fig. 1), which is such that $Ra = Ra_{\mathrm{loc}} = 14.3552$ when x is large. Such a definition presents a very simple means of predicting where the boundary layer becomes unstable by determining numerically where $Ra_{\mathrm{loc}} = 14.3552$ whenever $Ra > 14.3552$. This yields a value of ξ which we denote by ξ_{loc}. This rough local Rayleigh number method will be compared with full solutions of (34) and (35) later, but it is clear that the critical value of ξ will decrease as Ra increases.

Equations 34 and 35 were solved using the same Keller-box as described earlier, and both these equations and those for the basic temperature profile were solved simultaneously. A steplength of 0.1 was taken in the η-direction with $\eta_{\max} = 10$, while different steplengths were used in the ξ direction because the critical time varies greatly with the value of the Rayleigh number. We introduced a localised change in the boundary temperature centred at a value of ξ denoted by ξ_i, which we call the initiation distance:

$$\Theta(\xi, \eta = 0) = \exp\left[-((\xi - \xi_i)/c)^2\right], \tag{36}$$

where the constant, c, which is measure of the spread of the disturbance, was usually taken to be ξ_i itself. For each value of Ra, the chosen value of ξ_i was roughly 10% of the estimated

critical value of ξ in order that the computed critical value is unaffected by changing ξ_i to smaller values (see Selim and Rees (2007a). A comprehensive set of simulations were run for a variety of values of Ra and the wavenumber, k.

Selim and Rees (2007a) investigated different ways in which the magnitude of the evolving disturbance might be measured: the surface rate of heat transfer, the maximum temperature and an energy functional. It was found that the energy functional yields the earliest onset criterion, possibly because it is a global measure of the strength of the disturbance. This conclusion was also found to be true in the plume stability analysis of Rees et al. (2008a). Therefore, for the present paper, we monitored the variation with ξ of E, defined by

$$E(\xi) = \int_0^\infty \Theta \, \mathrm{d}y = \frac{2\xi}{2\xi + 1} \int_0^\infty \Theta \, \mathrm{d}\eta. \tag{37}$$

Given that the disturbance is caused by a localised change in the surface boundary condition for Θ, the value of E will grow initially as the surface disturbance diffuses into the porous medium, but will soon begin to decay due to the fact that the boundary layer is stable. But once the layer becomes thermoconvectively unstable, E will begin to grow again. We determine the value of ξ at which E has a minimum, and this value is recorded as the position of incipient instability for the chosen values of Ra and k. In some cases E decays once more after an interval of growth, and this corresponds to restabilisation of the layer. So for a chosen Darcy–Rayleigh number, the Keller-box code is used for a large range of values of the wavenumber, and a neutral curve is constructed by determining where E attains its maxima and minima for each wavenumber. Representations of these curves are shown in Figs. 2 and 3.

Figure 2 depicts the neutral curves for the following values of the Darcy–Rayleigh number: 15, 16, 20, 30, 40, 50, 60 and 100. The minimum value of ξ (denoted by ξ_c) for each curve is denoted by a bullet, and the numerical values are given in Table 1. The region corresponding to linear instability for each curve lies above the depicted minima. When Ra is just above the smallest value (14.3552) which admits instability, then the critical distance is relatively large, as the basic boundary layer has to grow to almost its asymptotic thickness before instability can occur. For these cases instability occurs only within a small band of wavenumbers about the critical value.

As the Darcy–Rayleigh number increases, so the onset of convection takes place at locations which are closer to the leading edge. Moreover, the critical wavenumber also increases. This latter fact may be explained by appealing to the fairly general (though not entirely universal) observation that the critical modes of instability tend to have an aspect ratio that is close to unity. As instability arises closer to the leading edge where the boundary layer is thinner, so the critical wavelength will be correspondingly shorter. Hence the wavenumber tends to increase. Once Ra achieves the value of 100, the lower part of the neutral curve has adopted the standard 'tear drop' shape which is typical of developing boundary layers (see, for example, Selim and Rees (2007a) and Rees (2001), although, for larger values of ξ, where the boundary layer assumes constant thickness, the two branches of the curve become vertical, and these now delimit the unstable band of wavenumbers.

Table 1 also shows the variation of k_c/Ra and $\xi_c Ra$ with Ra. These are, respectively, the critical wavenumber and distance corresponding to a nondimensionalisation where the Darcy–Rayleigh number is set to unity (thereby yielding a different natural lengthscale, L) and the suction velocity is allowed to vary. Thus large values of Ra within the present nondimensionalisation correspond to small suction velocities in this alternative one. Therefore the limit of large values of Ra here is equivalent to having no suction in the alternative scenario, and the values of k_c/Ra and $\xi_c Ra$ should then tend to a finite non-zero limit as $Ra \to \infty$. These limiting values should also be exactly the values as were obtained by Selim and Rees

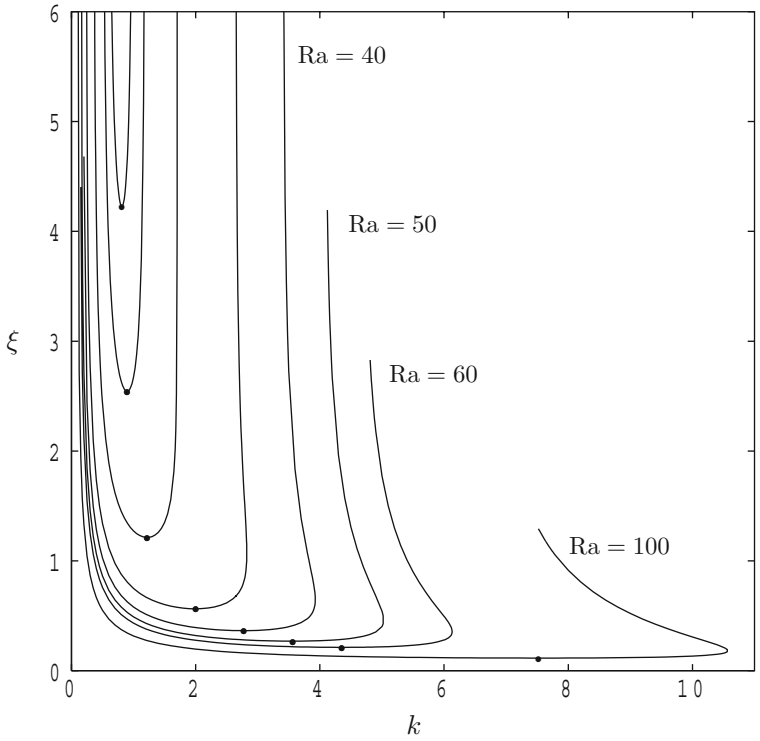

Fig. 2 Neutral curves determined by monitoring the behaviour of the energy functional, E. For $Ra = 15$ (*uppermost curve*), 16, 20, 30, 40, 50, 60 and 100 (*lowest curve*). Bullets mark the location of the respective minimum of each curve

(2007a) as their unsteady system is precisely equivalent to the unbounded Graetz problem in porous media without surface suction; it is these values that are quoted on the last line of Table 1. Figure 3 shows how the neutral curves of Fig. 2 are transformed when making the same shift in perspective; here the tendency towards a limiting curve as $Ra \to \infty$ may be seen easily.

Finally, we compare the critical values of the numerical simulations with the local Rayleigh number method described earlier. In Table 1 we list the appropriate values of ξ_{loc} and the ratio of these with the corresponding values of ξ_{c}. It shows that the critical value of ξ is always overestimated compared with the results of the numerical simulation. However, as Ra decreases towards 14.3552, the *relative* error in ξ_{loc} decreases although the absolute error increases. The improvement in the relative error arises because of the definition of the local Darcy–Rayleigh in terms of the shape of the large-ξ basic temperature profile.

5 Nonlinear Evolution

5.1 Preamble

In this section we consider the effect of introducing disturbances of $O(1)$ magnitude to determine whether the presence of the nonlinear terms alters any of the conclusions given above

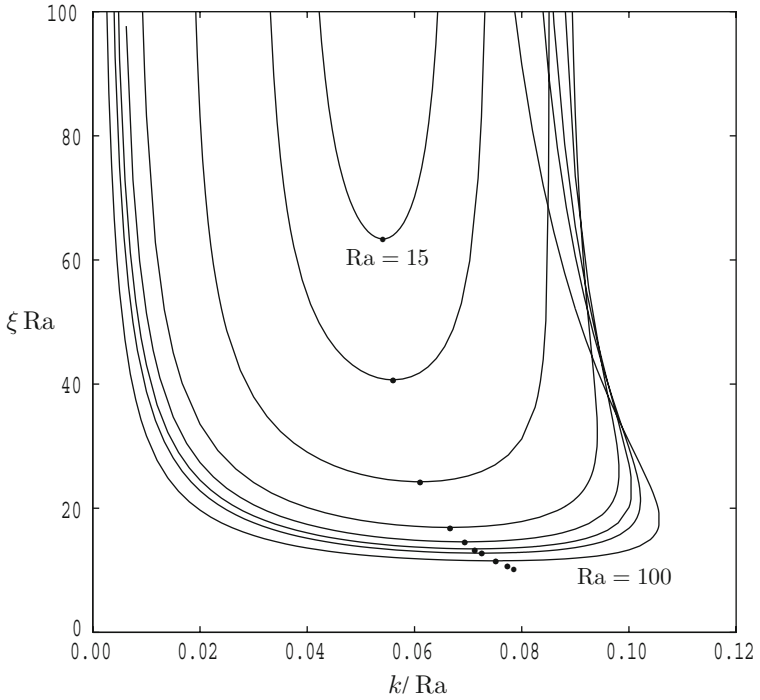

Fig. 3 Neutral curves determined by monitoring the behaviour of the energy functional, E. For $Ra = 15$ (*uppermost curve*), 16, 20, 30, 40, 50, 60 and 100 (*lowest curve*). Bullets mark the location of the respective minimum of each curve. Isolated bullets denote $Ra = 200$ and 400

Table 1 Critical values as a function of Ra and comparisons with a local Rayleigh number analysis

Ra	k_c	ξ_c	k_c/Ra	$\xi_c Ra$	ξ_{cloc}	ξ_{loc}/ξ_c
14.3552	0.7589					
14.5	0.76976	9.4406			10.2533	1.086
15	0.81169	4.2260	0.05411	63.390	4.7714	1.129
16	0.89631	2.5430	0.05602	40.641	2.9765	1.170
20	1.2214	1.2136	0.06107	24.272	1.5150	1.248
30	1.9998	0.56380	0.06666	16.914	0.74824	1.327
40	2.7762	0.36498	0.06941	14.599	0.49906	1.367
50	3.5638	0.26939	0.07128	13.369	0.37339	1.386
60	4.3521	0.21288	0.07253	12.773	0.29786	1.399
100	7.5217	0.11544	0.07517	11.544	0.16346	1.416
∞	∞	0	0.07807	8.9018		

with regard to the onset of convection. There are various studies which have already presented different aspects of the nonlinear properties of related boundary layers. For example, Selim and Rees (2007b) considered an unsteady boundary layer which is completely equivalent to the present boundary layer when the Darcy–Rayleigh number is large. In that work it was found that such large disturbances did not cause subcritical growth (i.e. growth at a value

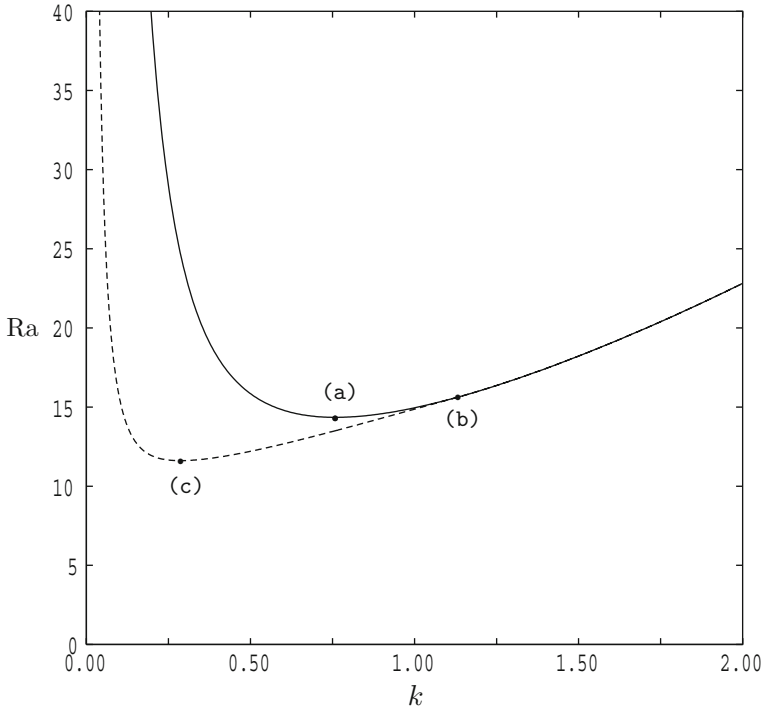

Fig. 4 Neutral curves for the Wooding (1960) problem. The continuous line denotes the linear stability curve. The dashed line denotes the limit of nonlinear solutions. Bullets denote the specific points: **a** the minimum of the linear curve; **b** the quartic point (i.e. where the nonlinear curve branches off the linear curve); **c** the nonlinear curve

of ξ which is smaller than that given by parabolic simulations of the linearised equations. However, nonlinear saturation and premature decay were found.

On the other hand, studies such as those of Homsy and Sherwood (1976) and Jones and Persichetti (1986), consider Darcy–Benard convection in layers with vertical throughflow, and these are exactly equivalent to vortex convection in the present large–ξ regime. Both these articles stress the presence of subcritical convection, by which is meant that strong convection can occur for values of the Darcy–Rayleigh number which are below that given by linearised theory, namely 14.3552. For the sake of illustrating the results of our computations, we have recalculated the linear and nonlinear neutral curves for this situation, and these are given in Fig. 4. The linearised (continuous) curve was found using a standard shooting technique with a fourth-order Runge–Kutta basic solver, and the minimum value is labelled `(a)`. For each wavenumber the second (dashed) curve corresponds to the smallest value of *Ra* for which nonlinear convection exists. Thus, for any chosen wavenumber, the zero solution loses stability at the linear stability curve, whereupon is suffers either a supercritical bifurcation (for wavenumbers larger than that given by the point labelled, `(b)`, in Fig. 4) or a subcritical bifurcation for smaller wavenumbers. This point, which we term a quartic point, was obtained using a straightforward weakly nonlinear analysis to third order, where zero curvature was imposed in order to identify the transition from supercritical to subcritical bifurcations. When the bifurcation is subcritical, the solution curve eventually passes through a turning point which marks the limit of nonlinear solutions; the dashed curve in Fig. 4 shows

Table 2 Values of Ra and k corresponding to the labelled points in Fig. 4

	Ra	k
(a)	14.3552	0.7589
(b)	15.6308	1.1320
(c)	11.6132	0.2867

how this turning point varies with wavenumber. The minimum of this nonlinear stability curve is denoted by (c). The values of Ra and k corresponding to these three points are given in Table 2, where it is noted that the location of (c) is different from that given in Homsy and Sherwood (1976) and Pieters and Schuttelaars (2008) because the curve corresponds only to two-dimensional patterns.

In the light of the above observations our a priori expectation was that the nonlinear results of Selim and Rees (2007b) would be recovered when Ra is large, and that it should be possible to obtain nonlinear solutions when $Ra < 14.3552$ provided that the initial disturbance is sufficiently large.

5.2 Governing Equations

The governing equations for the fully nonlinear simulations were obtained by successive transformations of Eqs. (22) and (23) using the substitution, $x = Pe\,X$, formally letting $Pe \to \infty$ to obtain the boundary layer approximation, and then employing the continuous transformation given in (29). We obtain,

$$\frac{\partial^2 p}{\partial \eta^2} + \left(\frac{2\xi}{1+2\xi}\right)^2 \frac{\partial^2 p}{\partial y^2} = Ra\left(\frac{2\xi}{1+2\xi}\right)\frac{\partial \theta}{\partial \eta}, \tag{38}$$

$$\frac{\partial^2 \theta}{\partial \eta^2} + \left[\frac{2\xi}{1+2\xi} + \frac{2\eta}{(1+2\xi)^2}\right]\frac{\partial \theta}{\partial \eta} + \left(\frac{2\xi}{1+2\xi}\right)^2 \frac{\partial^2 \theta}{\partial y^2} + \left[\frac{\partial p}{\partial \eta} - Ra\left(\frac{2\xi}{1+2\xi}\right)\theta\right]\frac{\partial \theta}{\partial \eta} + \left(\frac{2\xi}{1+2\xi}\right)^2 \frac{\partial p}{\partial y}\frac{\partial \theta}{\partial y} = \frac{2\xi}{(1+2\xi)^2}\frac{\partial \theta}{\partial \xi}. \tag{39}$$

These equations were solved by first performing a spectral decomposition in the spanwise direction,

$$(p, \theta) = \tfrac{1}{2}(p_0, \theta_0) + \sum_{n=1}^{N} (p_n, \theta_n) \cos nky, \tag{40}$$

and then by employing a suitably extended version of the previously described Keller-box code, although we left the equations in the second-order form in η in order to make efficient use of CPU time. The coefficient functions, p_n and θ_n, remain functions of η and ξ. The number of modes used in all our calculations was $N = 12$, which yields a system of 26 second-order PDEs. The manner in which the nonlinear terms were dealt with are as described in Selim and Rees (2007b). The boundary conditions at $\eta = 0$ were taken to be

$$\theta_0 = 2, \quad \theta_1 = A\,\exp\left[-((\xi - \xi_i)/c)^2\right], \quad \theta_n = 0 \qquad (n \geq 2), \tag{41}$$

where A is the amplitude of the disturbance, while the pressure condition was that

$$\frac{\partial p_n}{\partial \eta} = Ra \left(\frac{2\xi}{2\xi + 1} \right) \theta_n \qquad \forall n. \tag{42}$$

The results of our numerical simulations are presented in two forms: (i) the rate of heat transfer due to each mode defined as

$$q_n(\xi) = \frac{\partial \theta_n}{\partial z} |_{z=0}, \tag{43}$$

and, (ii) as a 'heat transfer footprint', which we will define as the contours of the rate of heat transfer at the surface as a function of ξ and y:

$$Q(\xi, y) = \sum_{n=1}^{N} \frac{\partial \theta_n}{\partial z} |_{z=0} \cos nky. \tag{44}$$

When values of q_n are plotted, we show both the computed value of q_0, which is the mean rate of heat transfer for the vortices, and the corresponding value (denoted as q_b) when disturbances are absent: the comparison of these two curves shows by how much the instability has changed the mean rate of heat transfer. The above definition of Q may be seen not to involve the mean rate of heat transfer due to mode 0—this is because the chief aim is to visualise easily the induced pattern of convection.

5.3 Results for $Ra = 20$ and $k = 1$

The variations of q_n and Q for a fairly standard case are given in Figs. 5 and 6. Here we have chosen to use $Ra = 20$, $k = 1$ and $\xi_i = 1$ with the two disturbance amplitudes, $A = 0.001$ and $A = 0.5$. With regard to Fig. 4, this value of k corresponds to a very weakly subcritical bifurcation, but $Ra = 20$ is well above the linear critical value which is approximately 15. It is therefore no surprise that the resulting evolution with ξ yields a convection pattern with the same dominant wavenumber as the initial disturbance. In Fig. 5 we see that the values of q_n decrease in magnitude fairly rapidly as n increases, suggesting that this is a solution with only a moderate nonlinearity. We also see that the value of ξ at which vortices begin to

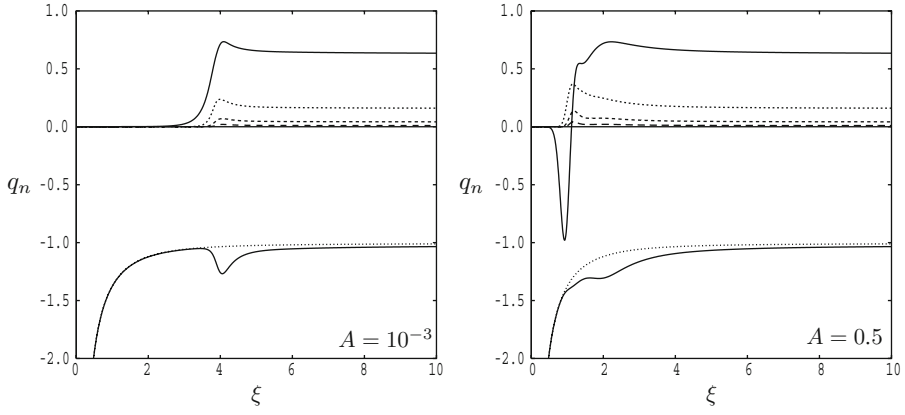

Fig. 5 Values of the modal surface rate of heat transfer, q_n, for $n = 0, \ldots 4$. The parameters are: $Ra = 20$, $k = 1$ and $\xi = 1$. In the lower part of each frame the continuous line denotes q_0, while the dotted line corresponds to the basic state, for comparison. In the upper part, the continuous line denotes q_1, long dashes are q_2, intermediate dashes are q_3 and short dashes are q_4; this convention applies to all figures of this type

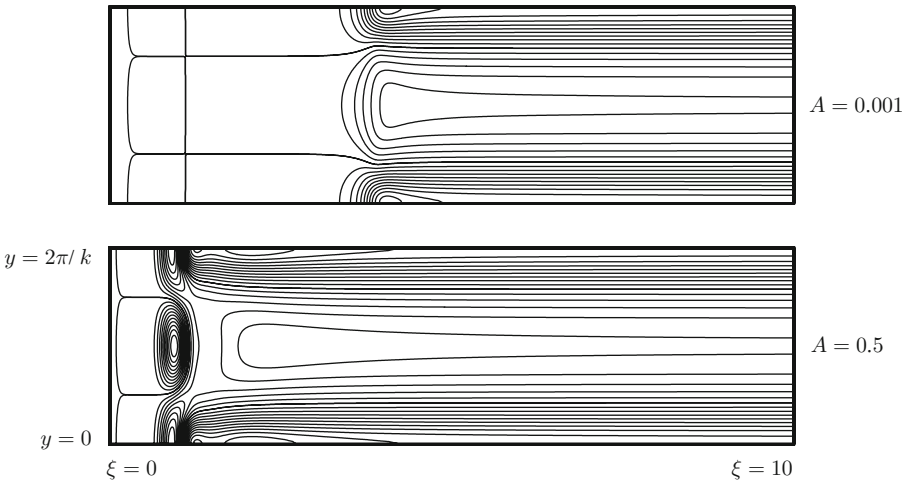

Fig. 6 Surface heat transfer profiles. Contours of Q are in increments of 0.1. The parameters are $Ra = 20$, $k = 1.0$ with $A = 0.001$ and 0.5

have an $O(1)$ effect depends strongly on the amplitude of the disturbance. Small values of A delay the overt appearance of instability, while sufficiently large amplitudes bring it forward to values of ξ that are close to the neutral curves shown in Fig. 2. These observations are also consistent with the view presented by Fig. 6 where one disturbance wavelength is shown.

No doubt there are many almost identical cases that could be presented when the wavenumber is close to or above the linear critical value (marked (a) in Fig. 4), but more interesting phenomena may be obtained when the wavenumber is closer to the nonlinear minimum (marked (c) in Fig. 4) where there is the possibility of deep subcriticality.

5.4 Results for $Ra = 20$ and $k = 0.3$

Figure 7 displays the case, $Ra = 20$, $k = 0.3$ and $\xi_i = 1$ for six different disturbance amplitudes. When $A = 0.001$, mode 3 eventually dominates, even though the initial disturbance is, by definition, of the form of mode 1. However, nonlinear interactions of mode 1 with itself soon yields a cascade of higher modes each with a very small amplitude. Given that they have the respective wavenumbers of 0.6 and 0.9, Fig. 4 suggests that both modes 2 and 3 might also be linearly unstable, although mode 3 has a lower critical Rayleigh number. Therefore, in the present scenario, it appears that mode 3 has the faster growth rate, and therefore it eventually dominates. The appropriate frame in Fig. 8 shows quite clearly how the modal pattern changes as ξ increases, and how rapidly the strongly nonlinear mode 3 appears.

When A rises to the value 0.1 a more intricate modal competition happens with mode 3 dominating eventually. However, the decaying q_1 and q_2 curves also oscillate about zero, and Fig. 8 shows that this is equivalent to decaying oscillations in the location of the axes of the vortices. While this might seem to be a somewhat strange phenomenon, it must be remembered that periodic convection patterns which are bounded either above or below by a solid surface may be destabilised by disturbances which change the position of a single cell. In such a case, the two cells which are now closer together than they were previously may attract one another by an entrainment mechanism which is similar to the Coandă effect

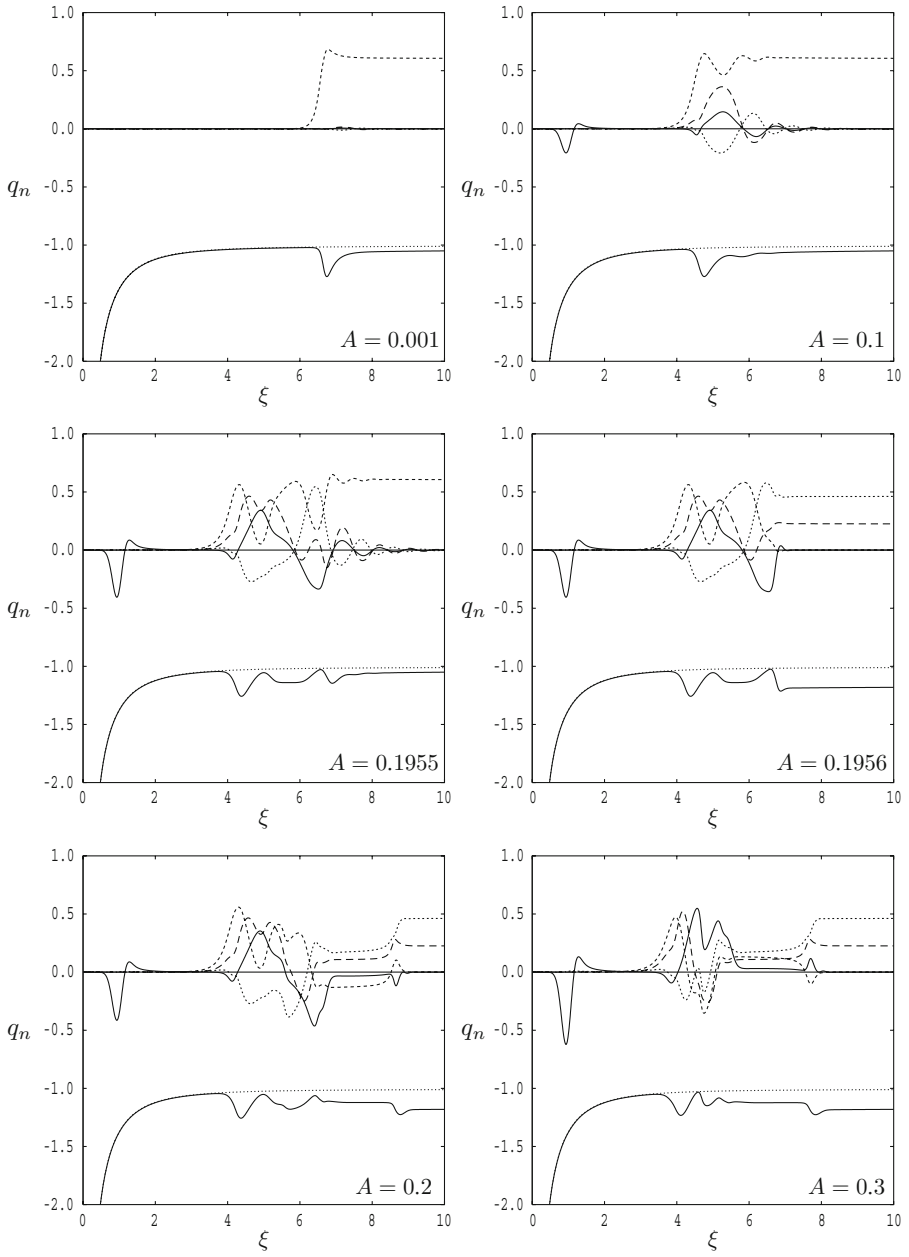

Fig. 7 Values of the modal surface rate of heat transfer, q_n, for $n = 0, \ldots 4$. The parameters are: $Ra = 20$, $k = 0.3$ and $\xi_i = 1$

in aerodynamics; see Banu et al. (1998) and Brambles and Rees (2007) for examples in the porous media context. Clearly, when $A = 0.1$, this entrainment process is not strong enough for cell merging and the ultimate fate is a mode 3 pattern again.

However, when A rises to the value 0.1956, the amplitude of the 'bounce' is too large, and we see a sudden change from a mode 3 final state when $A = 0.1955$ to a mode 2 final state

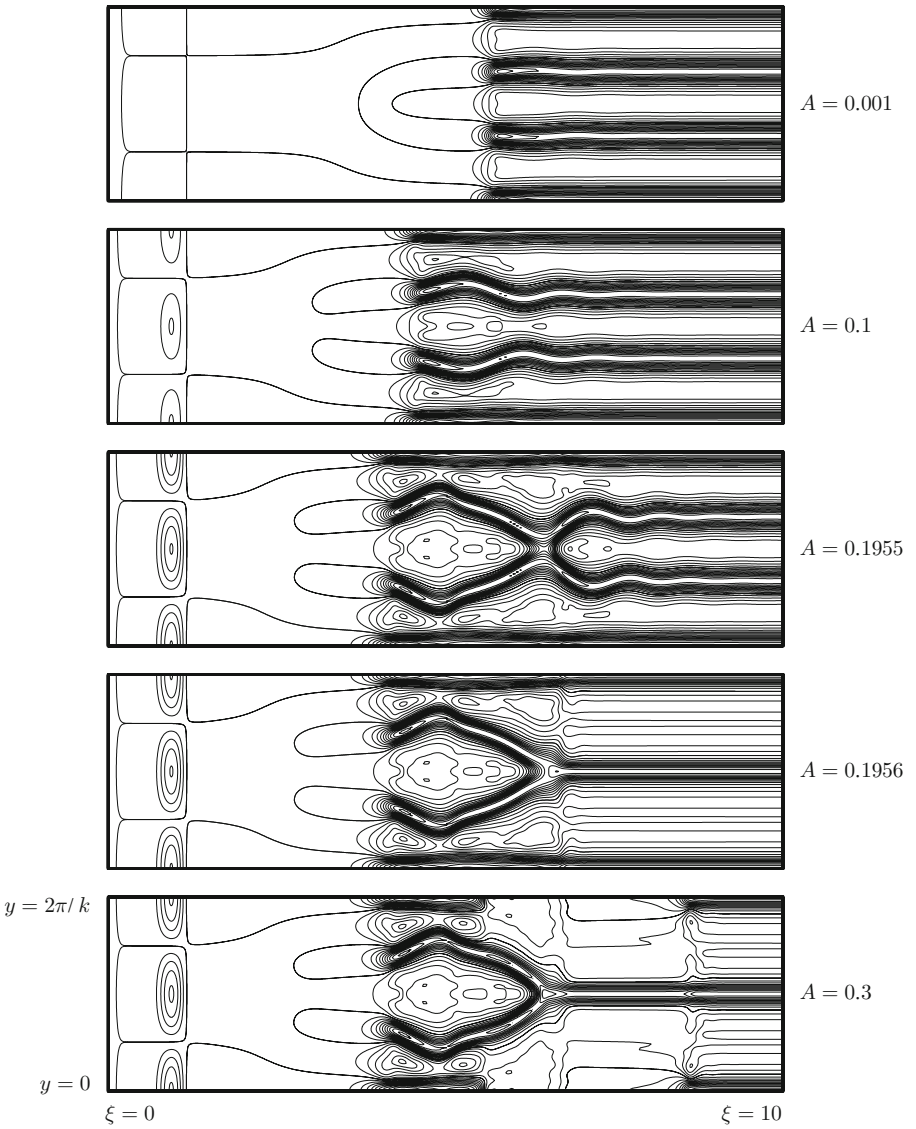

Fig. 8 Surface heat transfer profiles. Contours of Q are in increments of 0.1. The parameters are $Ra = 15$, $k = 0.3$ and $\xi_i = 1$

when $A = 0.1956$. At slightly higher disturbance amplitudes, a further transition occurs to a situation where the values of q_1 through to q_4 are of roughly equal magnitudes for quite a range of values of ξ before a mode 2 solution eventually dominates. This new intermediate state, which is clearly only just unstable, consists of an isolated region of high heat transfer, and which would technically be classed as mode 1. The associated flow pattern would then take the form of rather squat vortices which are approximately $\pi/0.3 \simeq 10$ wide in the y-direction but are only $-\ln(0.1) \simeq 2.3$ high. It is interesting to note the behaviour of the mean heat transfer curve, q_0, as one regime yields to the next, for while $|q_0|$ is clearly larger

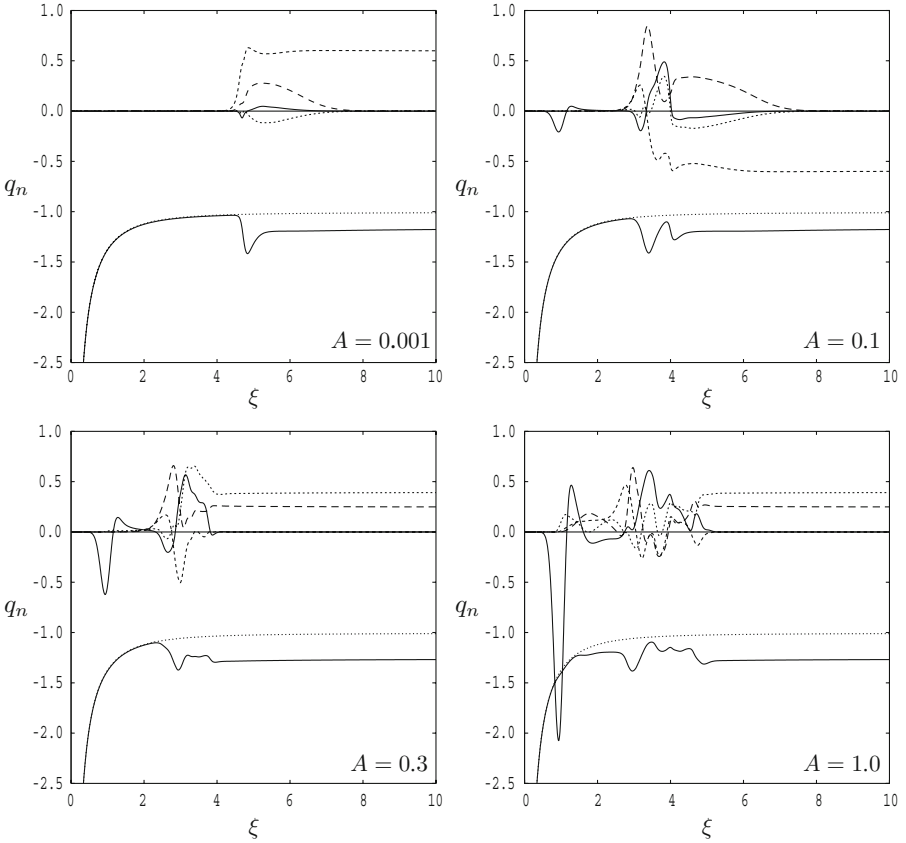

Fig. 9 Values of the modal surface rate of heat transfer, q_n, for $n = 0, \ldots 4$. The parameters are: $Ra = 25$, $k = 0.3$ and $\xi_i = 1$

than its equivalent for the basic state, it becomes larger again once the isolated vortex pattern destabilises to the mode 2 state.

5.5 Results for $Ra = 25$ and $k = 0.3$

Figures 9 and 10 correspond to the case, $Ra = 25$ and $k = 0.3$. The value of the Darcy–Rayleigh number is higher than in the case presented in Figs. 7 and 8, and therefore the most obvious consequence is that the ultimate value of q_0 is larger in magnitude, reflecting the fact that convection is stronger. Indeed, a comparison of corresponding frames in Figs. 7 and 9 shows that strong convection is attained earlier for the larger value of Ra, which is not surprising. Although this larger value of Ra also has a transition from mode 3 to mode 2 as the disturbance amplitude, A, becomes larger, there are various significant differences between when $Ra = 20$ and when $Ra = 25$. The increased magnitude of the buoyancy force due to the larger value of the Darcy–Rayleigh number causes a stronger modal interaction when $A = 0.1$ than for the corresponding when $Ra = 20$. The flow eventually settles down to a mode 3 state, as it does when $A = 0.001$, but with the opposite sign. This may be seen in Fig. 10 as a change in the phase of of the convection pattern. The modal interaction process

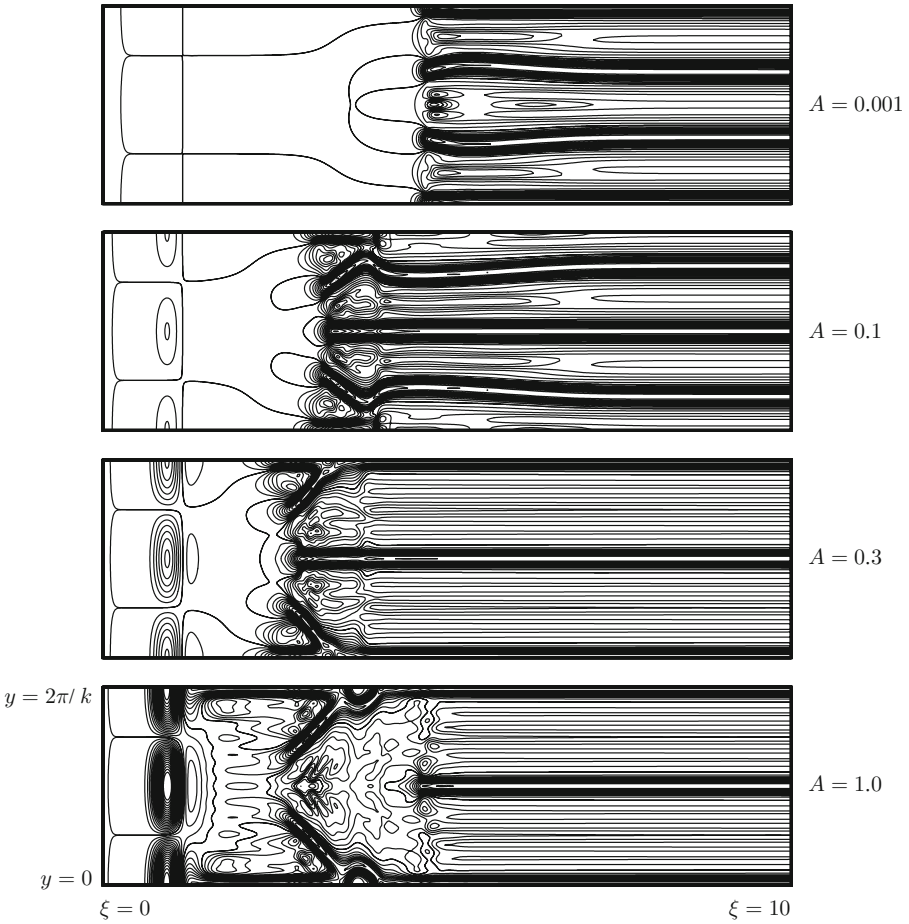

Fig. 10 Surface heat transfer profiles. Contours of Q are in increments of 0.1. The parameters are $Ra = 25$, $k = 0.3$ and $\xi_i = 1$

is still very sensitive to changes in the value of A, and we cannot guarantee that there is a sudden transition from a positive value of q_3 to a negative one at some critical value of A. At larger values of A a mode 2 solution appears to dominate when ξ is large, but it is preceded by a very complicated modal exchange. This complexity is depicted in Fig. 10 where some fairly rapid cell merging may be seen. The detailed evolution of the heat transfer footprint near to $\xi = 3$ is changed greatly when A increases from 0.3 to 1.0.

5.6 Results for $Ra = 11.8$ and $k = 0.2867$

Finally, we have also attempted to obtain some solutions at Darcy–Rayleigh numbers below 14.3552, and one such case is shown in Fig. 11. This corresponds to the following parameters: $Ra = 11.8$, $k = 0.2867$, $\xi_i = 1$ and $A = 2$. The chosen values of Ra and k lie just above the minimum of the nonlinear marginal curve in Fig. 4, while the chosen amplitude had to be sufficiently large in order to obtain a vortex solution. Indeed, smaller values of A gave solutions where the basic state was recovered once the disturbance had decayed. At such a low

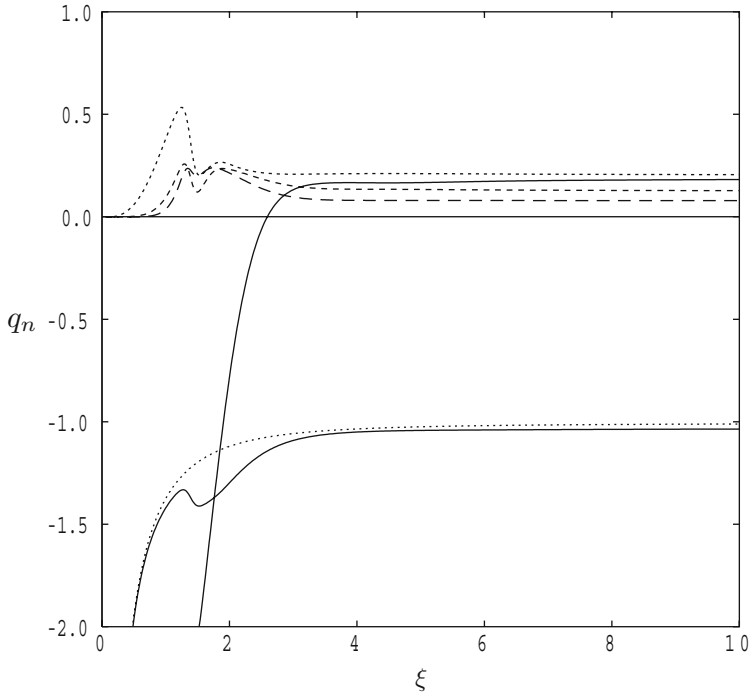

Fig. 11 Values of the modal surface rate of heat transfer, q_n, for $n = 0, \ldots 4$. The parameters are: $Ra = 11.8$, $k = 0.2867$, $\xi_i = 1$ and $A = 2$

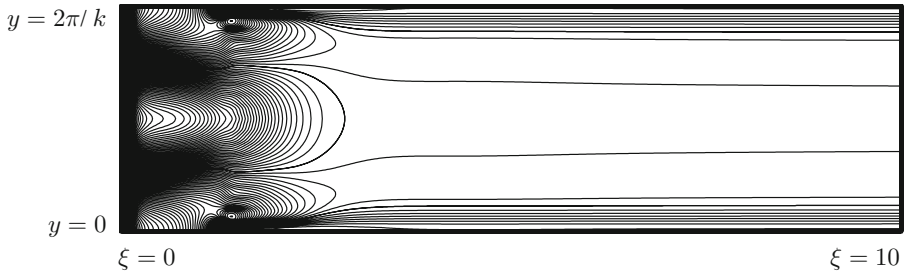

Fig. 12 Surface heat transfer profiles. Contours of Q are in increments of 0.1. The parameters are $Ra = 11.8$, $k = 0.2867$, $\xi_i = 1$ and $A = 2$

value of Ra the modal interactions are not strong, but nevertheless Fig. 11 shows that they produce a state where the first four modes have roughly comparable values of q_n, and therefore it is difficult to guess what the convection pattern looks like. The heat transfer footprint is shown in Fig. 12, and the large-ξ pattern consists of regions of low rates of heat transfer separated by relatively wide regions of high heat transfer; this situation is very similar to that depicted in Fig. 9 of Alloui et al. (2005). Further computations to very large values of ξ suggests that this pattern is quite stable, unlike the similar pattern found when $Ra = 20$, $k = 1$, $\xi_i = 1$ and $A = 0.3$, shown in Figs. 7 and 8, and which occurs between $\xi = 6$ and $\xi = 7$.

Space precludes the presentation of other solutions, such as flows at higher values of Ra or disturbances with different wavenumbers. But it is clear, even from this brief survey, that

the ultimate pattern of convection, as well as the manner of its evolution, depends quite strongly and sometimes quite sensitively on the values of governing parameters. Whereas the waviness of the cells shown in Fig. 8 might suggest a mechanism akin to the Ekhaus instability (noting that distance along the boundary layer here plays roughly the same role as time would in a traditional Ekhaus analysis), a full study of this would require a much larger number of modes with a smaller fundamental wavenumber in order to determine the effect of disturbances of the form of sideband modes, i.e. those with slightly different wavenumbers from that of the fundamental mode. It is highly likely that a more efficient numerical study would therefore require a full finite difference discretisation.

6 Conclusions

In this article, we have considered the thermoconvective instability with respect to vortex disturbances of the developing forced convection boundary layer flow over a horizontal surface with small-amplitude surface suction. A detailed linearised stability analysis was presented where the full parabolic partial differential equations for the disturbances were solved numerically. Neutral curves were obtained by monitoring the variation with ξ of an energy functional. The neutral curves were compared favorably with known limiting cases. This study was extended into the nonlinear regime using a spanwise spectral decomposition of the now large amplitude disturbances. The detailed evolution of vortices is surprisingly rich and provides many different phenomena: wavy vortices, sudden transitions between different convecting states, subcritical convection, sensitivity to initial conditions in some parameter regimes. Therefore our presentation of nonlinear convection can only be regarded as indicative of the complicated nature of modal selection mechanisms in a developing boundary layer.

References

Alloui, Z., Nguyen-Quang, T., Nguyen, T.H., Le Palec, G., Bournot, P.: Onset of convection in a porous cavity with vertical throughflow. In: Proceedings of the 12èmes Journées Internationales de Thermique, pp. 77–80, Tangiers, Morocco, November 2005

Banu, N., Rees, D.A.S., Pop, I.: Steady and unsteady convection in rectangular porous cavities with internal heat generation. In: Proceedings of the 11th International Heat Transfer Conference, vol. 4, pp. 375–380, Kyongju, Korea, August 1998

Brambles, O.J., Rees, D.A.S.: Curved free convection plume paths in porous media. Időjárás. Q. J. Hung. Meteorol. Serv. **111**, 109–121 (2007)

Ennis-King, J.P., Preston, I., Paterson, L.: Onset of convection in anisotropic porous media subject to a rapid change in boundary conditions. Phys. Fluids **17**, 084107.1–084107.15 (2005)

Hassanien, I.A., Salama, A.A., Moursy, N.M.: Inertia effect on vortex instability of horizontal natural convection flow in a saturated porous medium with surface mass flux. Int. Commun. Heat Mass Transf. **31**, 741–750 (2004)

Homsy, G.M., Sherwood, A.E.: Convective instabilities in porous media with through flow. AIChE J. **22**, 168–174 (1976)

Jang, J.-Y., Lie, K.-N., Chen, J.-L.: The influence of surface mass flux on vortex instability of a horizontal mixed convection flow in a saturated porous medium. Int. J. Heat Mass Transf. **38**, 3305–3311 (1995)

Jones, M.C., Persichetti, J.M.: Convective instability in packed beds with throughflow. AIChE J. **32**, 1555–1557 (1986)

Khalili, A., Shivakumara, I.S.: Onset of convection in a porous layer with net through-flow and internal heat generation. Phys. Fluids **10**, 315–317 (1998)

Khalili, A., Shivakumara, I.S.: Non-Darcian effects on the onset of convection in a porous layer with throughflow. Transp. Porous Media **53**, 245–263 (2003)

Khalili, A., Shivakumara, I.S., Suma, S.P.: Convective instability in superposed fluid and porous layers with vertical throughflow. Transp. Porous Media **51**, 1–18 (2003)
Kim, M.C., Choi, C.K., Yoon, D.-Y.: Analysis of the onset of buoyancy-driven convection in a water layer formed by ice melting from below. Int. J. Heat Mass Transf. **52**, 5097–5101 (2008)
Nield, D.A.: Convective instability in packed beds with throughflow. AIChE J. **33**, 1222–1224 (1986)
Nield, D.A.: Convection in a porous medium with inclined temperature gradient and vertical throughflow. Int. J. Heat Mass Transf. **41**, 241–243 (1998)
Nouri-Borujerdi, A., Noghrehabadi, A.R., Rees, D.A.S.: The linear stability of a developing thermal front in a porous medium: The effect of local thermal nonequilibrium. Int. J. Heat Mass Transf. **50**, 3090–3099 (2007)
Pieters, G.J.M., Schuttelaars, H.M.: On the nonlinear dynamics of a saline boundary layer formed by throughflow near the surface of a porous medium. Phys. D Nonlinear Phenom. **237**(23), 3075–3088 (2008)
Plato, R.: Concise Numerical Mathematics. American Mathematical Society Bookstore, Providence, Rhode Island, USA (2003)
Rees, D.A.S.Thermal boundary layer instabilities in porous media: a critical review. In: Ingham, D.B., Pop, I. (eds.) Transport Phenomena in Porous Media, pp. 233–259. Pergamon, NY, USA (1998)
Rees, D.A.S.: Vortex instability from a near-vertical heated surface in a porous medium. I Linear theory. Proc. R. Soc. Lond. A **457**, 1721–1734 (2001)
Rees, D.A.S: Recent advances in porous medium thermal boundary layer instabilities. In: Ingham, D.B., Pop, I. (eds.) Transport Phenomena in Porous Media II, pp. 54–81. Pergamon, NY, USA (2002)
Rees, D.A.S., Storesletten, L.: The linear instability of a thermal boundary layer with suction in an anisotropic porous medium. Fluid Dyn. Res. **30**, 155–168 (2002)
Rees, D.A.S., Postelnicu, A., Bassom, A.P.: The linear vortex instability of the near-vertical line source plume in porous media. Transp. Porous Media **74**, 221–238 (2008a)
Rees, D.A.S., Selim, A., Ennis-King, J.P.: The instability of unsteady boundary layers in porous media. In: Vadasz, P. (ed.) Emerging Topics in Heat and Mass Transfer in Porous Media, pp. 85–110. Springer, NY, USA (2008b)
Riahi, D.N.: Nonlinear convection in a porous layer with permeable boundaries. Int. J. Non-Linear Mech. **24**, 459–463 (1989)
Riaz, A., Hesse, M., Tchelepi, H.A., Orr, F.M.: Onset of convection in a gravitationally unstable diffusive boundary layer in porous media.. J. Fluid Mech. **548**, 87–111 (2006)
Selim, A., Rees, D.A.S.: The stability of a developing thermal front in a porous medium. I. Linear theory. J. Porous Med. **10**, 1–15 (2007)
Selim, A., Rees, D.A.S.: The stability of a developing thermal front in a porous medium. II. Nonlinear theory. J. Porous Med. **10**, 17–33 (2007)
Shivakumara, I.S.: Boundary and inertia effects on convection in porous media with throughflow. Acta Mech. **137**, 151–165 (1999)
Shivakumara, I.S., Khalili, A.: On the stability of double diffusive convection in a porous layer with throughflow. Acta Mech. **152**, 165–175 (2001)
Shivakumara, I.S., Sureshkumar, S.: Convective instabilities in a viscoelastic-fluid-saturated porous medium with throughflow. J. Geophys. Eng. **4**, 104–115 (2007)
Shivakumara, I.S., Sureshkumar, S.: Effects of throughflow and quadratic drag on the stability of a doubly diffusive Oldroyd-B fluid-saturated porous layer. J. Geophys. Eng. **5**, 268–280 (2008)
Storesletten, L., Rees, D.A.S.: The influence of higher-order effects on the linear instability of thermal boundary layer flow in porous media. Int. J. Heat Mass Transf. **41**, 1833–1843 (1998)
Sutton, F.M.: Onset of convection in a porous channel with net through flow. Phys. Fluids **13**, 1931–1934 (1970)
van Duijn, C.J., Pieters, G.J.M., Wooding, R.A., van der Ploeg, A.: Stability criteria for the vertical boundary layer formed by throughflow near the surface of a porous medium In: Raats, P.A.C., Smiles, D., Warrick, A.W. (eds.) Environmental Mechanics—Water, Mass and Energy Transfer in the Biosphere—The Philip Volume, Geophysical Monograph, vol. 129. American Geophysical Union, Washington, DC (2002)
Wooding, R.A.: Rayleigh instability of a thermal boundary layer flow through a porous medium. J. Fluid Mech. **9**, 183–192 (1960)
Wooding, R.A.: Variable-density saturated flow with modified Darcy's law: The salt lake problem and circulation. Water Resour. Res. **43** (article no. W02429) (2007)
Wooding, R.A., Tyler, S.W., White, I.: Convection in groundwater below an evaporating salt lake. I. Onset of instability. Water Resour. Res. **33**, 1199–1218 (1997a)
Wooding, R.A., Tyler, S.W., White, I., Anderson, P.A.: Convection in groundwater below an evaporating salt lake. II. Evolution of fingers or plumes. Water Resour. Res. **33**, 1219–1228 (1997b)
Yoon, D.Y., Kim, D.S., Choi, C.K.: Convective instability in packed beds with internal heat sources and throughflow. Korean J. Chem. Eng. **15**, 341–344 (1998)